Assembling a Ring-Shaped Crystal in a Microfabricated Surface Ion Trap

Boyan Tabakov, Francisco Benito, Matthew Blain, Craig R. Clark, Susan Clark, Raymond A. Haltli, Peter Maunz, Jonathan D. Sterk, Chris Tigges, and Daniel Stick

Phys. Rev. Applied **4**, 031001 — Published 1 September 2015

DOI: 10.1103/PhysRevApplied.4.031001

Assembling a ring-shaped crystal in a microfabricated surface ion trap

Boyan Tabakov,[1,2] Francisco Benito,[1] Matthew Blain,[1] Craig R. Clark,[1] Susan Clark,[1] Raymond A. Haltli,[1] Peter Maunz,[1] Jonathan D. Sterk,[1] Chris Tigges,[1] and Daniel Stick[1,2]

[1] *Sandia National Laboratories, P.O. Box 5800 Albuquerque, NM 87185-1082*

[2] *Center for Quantum Information and Control, University of New Mexico, MSC 074220, Albuquerque, NM 87131-0001*

We report on experiments with a microfabricated surface trap designed for confining a chain of ions in a ring. Uniform ion separation over most of the ring is achieved with a rotationally symmetric design and by measuring and suppressing undesired electric fields. After reducing stray fields, the ions are confined primarily by a radiofrequency (rf) trapping pseudo-potential and their mutual Coulomb repulsion. Approximately 400 $^{40}Ca^{+}$ ions with an average separation of 9 μm comprise the ion crystal.

I. INTRODUCTION

The primary motivation for developing segmented surface ion traps [1] is to create structures that support the implementation of quantum algorithms, such as the proposed quantum charge-coupled device (QCCD) [2]. The fabrication techniques used to realize these surface traps also enable other geometries with desirable properties. In the case reported here, a trap with a nearly circularly symmetric rf pseudo-potential is designed to hold a ring-shaped chain of equidistant ions. Rings of trapped ions have been previously demonstrated for studying electron capture [3], storing protons and helium ions [4], and studying phase transitions and Coulomb crystals [5, 6]. In these cases the rings were large (>1 cm diameter) and were conventionally fabricated as multi-level structures. One of the primary technical challenges with rf Paul traps used for quantum information experiments is that the background electric field must be substantially eliminated so that the ions are trapped at the null of the rf oscillating field. This is routinely achieved in experiments with few ions, since only a few electrodes are needed to cancel out an uncontrolled (but generally static) background electric field present over a small region. Achieving this over a much larger region with many ions is more difficult, since it requires commensurately more electrodes at a sufficient density to generate local compensating electric fields.

The objective of our experiment was to similarly to trap a ring of crystallized ions, but use a micro-fabricated surface trap with sufficiently numerous and dense control electrodes to minimize electric field deviations which disrupt the circular symmetry of the ion positions. The causes for such deviations include unavoidable design limitations (e.g. control electrode gaps cannot be made infinitely thin) as well as experimental imperfections (e.g. surface contaminants and fields from charges on the in-vacuum components). While a ring geometry is not topologically similar to the QCCD array because it lacks features necessary to shuttle ions in a 2-dimensional lattice, there are proposals to take advantage of long chains for quantum information processing [7, 8]. In addition this geometry enables other experiments from diverse fields. These include simulations and studies of Ising models with long chains [9], Hawking radiation [10], quantum phase transitions [11], time crystals [12], topological defects [13, 14], and the Aharonov-Bohm effect [15]. While requiring different and additional types of control, this diverse list of applications benefits from the electric field control we present in this Letter.

II. TRAP LAYOUT

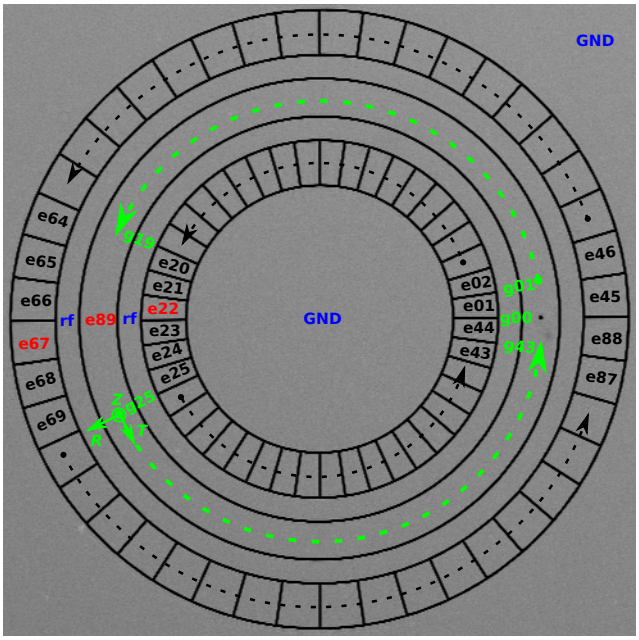

FIG. 1. Device layout and labeling. Of the 89 available control electrodes, 86 performed as expected (black labels and dashed arcs), while $e22$, $e67$, and $e89$ (red labels) are shorted to ground. The trapping volume is above the central control electrode, $e89$, and is designated by the green dashed arcs. The irregularities at the loading hole and the diametrically opposite location result from reduced control over the ion motion at these locations. The trapping sites are labeled "gXX" at the gaps in the control electrodes, with the loading hole at $g00$. An $R-T-Z$ reference frame is shown at $g25$.

A toroidal trapping volume is attained with the elec-

trode layout shown in Fig. 1. The trap comprises two rf electrodes with one control electrode between them and 88 axial control electrodes on either side, while all other top metal is grounded. The rf electrode provides the radial confinement for the ring of ions and the segmented control electrodes provide axial confinement. The circular symmetry of the trap makes it natural to work in a reference frame centered at a trapped ion (Fig. 1). In such a frame, the tangential (T) direction (positive counter-clockwise) is the analogue of the axial direction for a linear trap, the radial (R) direction points outward from the circle center, and Z is the direction perpendicular to the trap plane.

Many choices in the design are made to minimize undesired electric fields at the ions. First, any deviation from a continuous circle of the rf electrode or the rf ground (including control electrodes) introduces potential defects. To minimize these defects the rf lead extends outward from the ring on a buried metal level, and at a position 1.7 mm from the trap center it is routed to the top metal level to reduce capacitance. A similar routing strategy is used for the control electrodes and in general allows for the fabrication of more complicated traps with arbitrary electrode layouts. To realize access to islanded electrodes and hide the leads, four metal layers are used (Fig. 2).

A 10 μm diameter hole in the center control electrode enables backside loading. The gaps between electrodes are 7 μm, as small as possible relative to the ion height (<10%) in order to minimize perturbations to the rf potential, but large enough to avoid voltage breakdown and fabrication issues. Simulations show that the perturbations to the rf pseudo-potential due to gaps are dominated by the Coulomb repulsion between neighboring ions. Additionally, the insulators under the top electrodes are undercut so that charges that might build up on the surface are partially screened from the ions above (Fig. 2). Additional fabrication and experimental apparatus details can be found in [16].

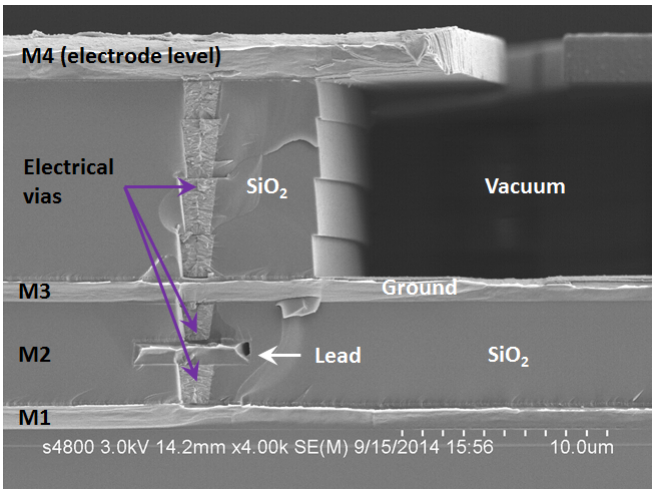

FIG. 2. Cross-sectional SEM of the trap, showing the four metal levels, interconnects, and insulators. The trap is fabricated using aluminum(Al)-1/2% copper (Cu) metalization, planarized silicon dioxide (SiO_2) inter-level dielectric (ILD), and vertical electrical connections using tungsten plug technology.

III. MEASURING AND CORRECTING STRAY FIELDS

Under these conditions, the distance between ions in the ring should be equal. However imaging an actual chain when control electrodes are all set to the same voltage (0 V) shows that the ion spacing is irregular. Ions are bunched in several locations and absent from others, due to stray electric fields that break the circular symmetry. Undesired electric fields near an ion trap can result from various sources, including laser charging on the trap surface, contaminants, imperfections in fabrication, and uncontrolled charges elsewhere in the vacuum chamber. These fields can vary in magnitude at the level of several thousand V/m [17] and can be reduced by applying compensating voltages to the control electrodes. A procedure to fully eliminate the electric fields at N locations would require simulations of the field throughout the ring produced by a voltage applied to each trap electrode. Then the actual field would be measured in three orthogonal directions at each location. Finally, the $3N$ linear equations which eliminate the electric fields would be solved and the corrective voltages applied to a minimum of $3N$ electrodes. The experiment described here focuses on correcting only the axial electric fields which are tangential to the ring, at a subset of 39 equidistant positions. We find that this spatial resolution (90 μm) is adequate for reducing the axial fields and achieving a near-uniform ion spacing, which is reasonable given the ion height of 82 μm.

For an arbitrary trapping location, the tangential component of the stray field is measured by scaling the control voltages and measuring the shift in position of a single trapped ion. For the tangential secular frequency ω_T of the ion, $\omega_T^2 \propto \alpha$ holds, where α is a scaling factor for a particular set of applied control voltages. The tangential component of the ion potential is $\phi_T = \frac{m}{2q}\omega_T^2 x^2 - E_T x$, where m is the ion mass, E_T is the stray field tangential component, q is the ion charge, and x is the ion's tangential displacement. At equilibrium, the displacement is a function of the stray field E_T: $x = \frac{E_T q}{m\omega_T^2}\frac{1}{\alpha}$. Displacement measurements for several α values along with a single secular frequency measurement are fitted to yield the tangential electric field value.

To assess the field components in the two orthogonal directions, we apply corrective fields in the R and Z directions to minimize secular motion excitation during a parametric scan [18, 19], and also minimize the correlation signal in a time of arrival experiment [20]. These were not subsequently corrected due to a lack of degrees of freedom, but were measured to vary by only ≈ 30 V/m across the the ring.

To achieve an equidistant chain over the region of interest the tangential field is first measured at 39 locations. For field correction, we assign one electrode per degree of freedom (39 electrodes). The field that a single electrode produces extends over the trap to all measurement locations and the system of equations is solved so that the total generated field (according to the model) cancels the measured field at each location. This is captured in the expression:

$$-\begin{pmatrix} E_1 \\ \vdots \\ E_{39} \end{pmatrix} = \begin{pmatrix} e_1^1 & \dots & e_1^{39} \\ \vdots & \ddots & \vdots \\ e_{39}^1 & \dots & e_{39}^{39} \end{pmatrix} \begin{pmatrix} \alpha^1 \\ \vdots \\ \alpha^{39} \end{pmatrix},$$

where E_i is the measured tangential field at location i, e_i^j is the simulated tangential field at location i due to one volt on electrode j, and α^j is the actual voltage applied to electrode j. We apply the outlined measurement to ions trapped at locations $g00-g19$ and $g25-g43$ (see Fig. 1), inclusive. We exclude locations $g20-g24$ due to shorted electrodes and therefore an inability to correct the axial electric field. Measurements of the tangential field components, before and after correction (Fig. 3), show that the simultaneously applied correction contributes to reducing the tangential field at all measurement locations.

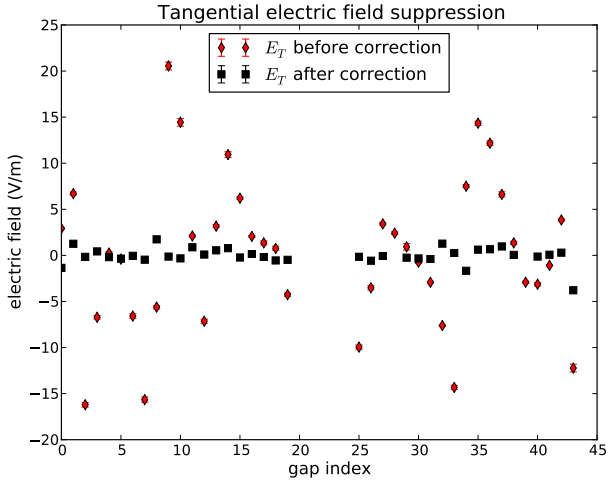

FIG. 3. Tangential field suppression before and after correction. The error bars (too small on this scale to be readily visible) are propagated from secular frequency and ion position uncertainties. The field at $g28$ and $g39$ is not calculated after correction due to difficulty in measuring the secular frequency.

A demonstration of the effect of tangential field reduction is shown by the long chain in Fig. 4, obtainable only after applying the correction. The magnification of the imaging system balances the competing requirements of individual ion resolution while capturing a large area. An image with the ring center in a corner covers almost a quarter of the trapping volume. To image the whole

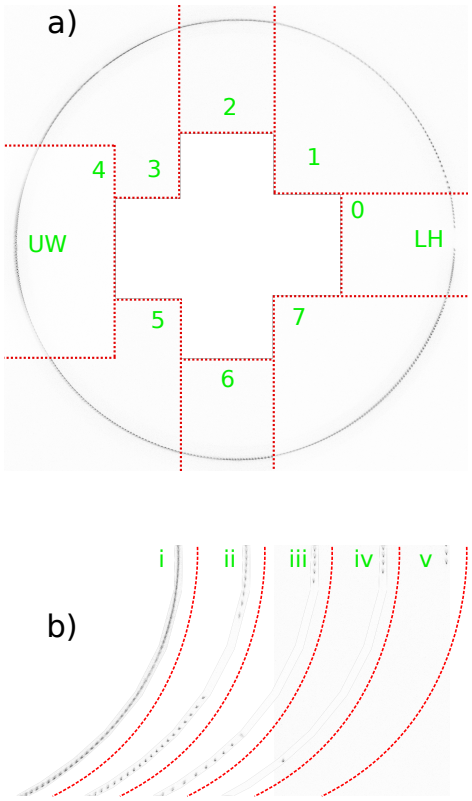

FIG. 4. **a)** A composite image of a full ring after correction. The stitched image comprises separate images of eight octants (labeled by the numbers shown). Without correcting the background fields, ions would primarily fall in an unwanted potential well (marked "UW") in proximity to the shorted electrodes $e22$ and $e67$ (see Fig. 1). With the correction, ions occupy the trapping volume except for above the loading hole (marked "LH"). Uneven illumination in octants 1, 2, 3, 5, 6, and 7 is due to the Gaussian profile of the cooling and repump beams, which are elliptically focused and cover the 1.3 mm diameter of the trap. In octant 4, uneven illumination is primarily a consequence of having limited control over electrodes $e22$ and $e67$, thus preventing field measurement and subsequent correction. The chain interruption at the loading hole is due to deficiencies in the model used to calculate the correction. **b)** Scaling the correction from 100% (label i) to 0% (label v) in 25% steps. As the corrective voltage decreases, the irregularities in the imaged segment increase.

chain, overlapping images are taken in each octant as the camera is moved in 45° increments along the circle. The obtained images are composed manually because there is no feature to reference the chain to, and an ion may be lost during this process and change the chain. To numerically assess the tangential field homogeneity at intermediate locations between the electrode gaps after stray field suppression, we analyze images in which all ions are resolved. The ion spacing is plotted (Fig. 5) for octants 5, 6, and 7. In the rest of the octants the ions were not well resolved due to cooling and imaging imperfections.

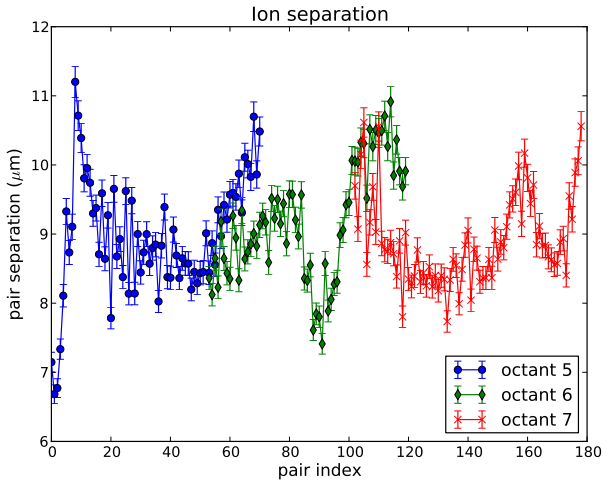

FIG. 5. Ion separation in three neighboring octants for which all ions are resolved. Overlap is inferred from the composite image of the full ring (Fig. 4). Imaging system and cooling beam imperfections prevent resolving all ions in the remaining five octants. The error bars are based on the uncertainty of the total magnification, but the positions are not corrected for aberrations at the edge of the collection optic.

IV. TRAP PERFORMANCE

The modeled pseudo-potential minimum is a circle of radius 624 μm at 82 μm above the trap surface. The model is created by meshing the surface geometry with CUBIT [21], feeding the mesh to CPO [22] for electric field estimation, and manipulating the calculated field with Mathematica for parameter extraction. For 400 ions spaced at 10 μm, the generated trapping strength is $\omega_T/2\pi = 360$ kHz for each ion. A 10 μm diameter loading hole is chosen because it only deforms the pseudo-potential with a 9 kHz local trapping potential, significantly smaller than the Coulomb potential between ions. Due to computational complexity, this consideration is not reflected in the large scale simulation used to obtain the correction, resulting in the observed gap in the chain at the loading hole after correction.

Away from the loading hole, the tangential secular frequency (ω_T) predicted by the simulations agreed with measurement to within a few percent. From measured values of $\omega_R/2\pi = 2.12$ MHz and $\omega_Z/2\pi = 2.17$ MHz, the rf voltage amplitude is estimated to be 80 V (drive frequency $\Omega/2\pi = 52.9$ MHz). This corresponds to a trap depth of 17 meV and provides sufficiently long ion lifetimes, observed up to 7 hours for a single ion in a well. While the ion chain is persistent on the order of hours, individual ions in the chain can be lost after minutes. Single ion control was also demonstrated by shuttling an ion in excess of 10^4 times around the ring consecutively without loss. A heating rate of 0.95(20) quanta/ms was measured on the tangential COM mode using the sideband ratio technique [23], for $\omega_T \approx 2\pi \times 0.9$ MHz, and could be improved with cleaning [16].

In many instances we are able to roughly correlate the stray field direction with the presence of particulate contaminants on the trap surface. We attribute this to particle charging due to the short wavelength lasers [24]. Particle locations were confirmed for selected locations by scattering light off the trap surface and independently by imaging the trap immediately after removing it with scanning electron microscopy (SEM). The tangential fields remain persistent over experimentally relevant durations of time. Observing ten different sites away from the loading hole over the period of one month, a maximum electric field change of 3.4 V/m was observed. The temporal change is greater near the loading hole due to exposure to the calcium source and ultraviolet photoionization lasers. Given that the automated measurement procedure takes hours, we conclude that the field correction procedure is a reasonable method for engineering an arbitrary field, in our case a corrective one, over a large trapping volume.

V. CONCLUSION

In this work a ring shaped surface trap is demonstrated and characterized by storing about 400 ions with near-uniform spacing over ∼90% of the ring. Equidistant spacing is achieved by measuring and reducing the axial electric fields at a 90 μm period around the ring, setting a long-range length scale (exceeding the 9 μm ion spacing) for the background electric fields. Achieving this uniformity is important for experiments requiring long chains of ions with circular boundary conditions, and could be improved by eliminating macroscopic surface contaminants and further reducing the size of the loading hole or positioning it under the gap between electrodes.

VI. ACKNOWLEDGMENTS

BT thanks Hartmut Häffner for ultra high vacuum advice, Kevin Fortier for help with lasers, and Jonathan Mizrahi for useful theoretical discussions.

Sandia National Laboratories is a multi-program laboratory managed and operated by Sandia Corporation, a wholly owned subsidiary of Lockheed Martin Corporation, for the US Department of Energy's National Nuclear Security Administration under contract DE-AC04-94AL85000 This work is part of the Multi-Qubit Coherent Operations (MQCO) program supported by the Intelligence Advanced Research Projects Activity (IARPA).

[1] M. D. Hughes, B. Lekitsch, J. A. Broersma, and W. K. Hensinger, Microfabricated ion traps, Contemporary Physics **52**, 505 (2011).

[2] D. Kielpinski, C. Monroe, and D. J. Wineland, Architecture for a large-scale ion-trap quantum computer, Nature **417**, 709 (2002).

[3] F. Bliek, R. Hoekstra, and R. Morgenstern, Ion storage at ev energies in an octopole ring, Hyperfine Interactions **99**, 193 (1996).

[4] D. A. Church, Storage - ring ion trap derived from the linear quadrupole radiofrequency mass filter, J. Appl. Phys. **40**, 3127 (1969).

[5] T. Schätz, U. Schramm, and D. Habs, Crystalline ion beams, Nature **412**, 717 (2001).

[6] M. Marciante, C. Champenois, A. Calisti, and M. Knoop, Structural phase transitions in multipole traps, Appl. Phys. B **107**, 1117 (2012).

[7] G.-D. Lin, S.-L. Zhu, R. Islam, K. Kim, M.-S. Chang, S. Korenblit, C. Monroe, and L.-M. Duan, Large-scale quantum computation in an anharmonic linear ion trap, EPL (Europhysics Letters) **86**, 60004 (2009).

[8] S. C. Doret, J. M. Amini, K. Wright, C. Volin, T. Killian, A. Ozakin, D. Denison, H. Hayden, C.-S. Pai, R. E. Slusher, and A. W. Harter, Controlling trapping potentials and stray electric fields in a microfabricated ion trap through design and compensation, New J. Phys. **14**, 073012 (2012).

[9] K. Kim, M.-S. Chang, S. Korenblit, R. Islam, E. E. Edwards, J. K. Freericks, G.-D. Lin, L.-M. Duan, and C. Monroe, Quantum simulation of frustrated Ising spins with trapped ions, Nature **465**, 590 (2010).

[10] B. Horstmann, B. Reznik, S. Fagnocchi, and J. I. Cirac, Hawking radiation from an acoustic black hole on an ion ring, Phys. Rev. Lett. **104**, 250403 (2010).

[11] E. Shimshoni, G. Morigi, and S. Fishman, Quantum zigzag transition in ion chains, Phys. Rev. Lett. **106**, 010401 (2011).

[12] T. Li, Z.-X. Gong, Z.-Q. Yin, H. T. Quan, X. Yin, P. Zhang, L.-M. Duan, and X. Zhang, Space-time crystals of trapped ions, Phys. Rev. Lett. **109**, 163001 (2012).

[13] H. Landa, S. Marcovitch, A. Retzker, M. B. Plenio, and B. Reznik, Quantum coherence of discrete kink solitons in ion traps, Phys. Rev. Lett. **104**, 043004 (2010).

[14] H. Landa, A. Retzker, T. Schaetz, and B. Reznik, Entanglement generation using discrete solitons in Coulomb crystals, Phys. Rev. Lett. **113**, 053001 (2014).

[15] A. Noguchi, Y. Shikano, K. Toyoda, and S. Urabe, Aharonov - Bohm effect in the tunnelling of a quantum rotor in a linear Paul trap, Nature Communications **5** (2014).

[16] See Supplemental Material at [URL to be supplied] for a description of the experimental setup and trap fabrication.

[17] C. R. Clark, C. W. Chou, A. R. Ellis, J. Hunker, S. A. Kemme, P. Maunz, B. Tabakov, C. Tigges, and D. L. Stick, Characterization of fluorescence collection optics integrated with a microfabricated surface electrode ion trap, Phys. Rev. Applied **1**, 024004 (2014).

[18] S. Narayanan, N. Daniilidis, S. A. Möller, R. Clark, F. Ziesel, K. Singer, F. Schmidt-Kaler, and H. Häffner, Electric field compensation and sensing with a single ion in a planar trap, J. Appl. Phys. **110**, 114909 (2011).

[19] Y. Ibaraki, U. Tanaka, and S. Urabe, Detection of parametric resonance of trapped ions for micromotion compensation, Appl. Phys. B **105**, 219 (2011).

[20] D. J. Berkeland, J. D. Miller, J. C. Bergquist, W. M. Itano, and D. J. Wineland, Minimization of ion micromotion in a Paul trap, J. Appl. Phys. **83**, 5025 (1998).

[21] https://cubit.sandia.gov/.

[22] http://simion.com/cpo/.

[23] Q. A. Turchette, D. Kielpinski, B. E. King, D. Leibfried, D. M. Meekhof, C. J. Myatt, M. A. Rowe, C. A. Sackett, C. S. Wood, W. M. Itano, C. Monroe, and D. J. Wineland, Heating of trapped ions from the quantum ground state, Phys. Rev. A **61**, 063418 (2000).

[24] M. Harlander, M. Brownnutt, W. Hänsel, and R. Blatt, Trapped-ion probing of light-induced charging effects on dielectrics, New J. Phys. **12**, 093035 (2010).